Dielectric permittivity of sodium di(2-ethylhexyl)sulfosuccinate–H_2O–iso-octane microemulsions in terms of their microscopic structure

C. Robertus
*Department of Molecular Biophysics, Buys Ballot Laboratory, University of Utrecht, P.O. Box 80.000, 3508 TA Utrecht, The Netherlands**

J. G. H. Joosten
DSM Research B.V., Section FA-GF, P.O. Box 18, 6160 MD Geleen, The Netherlands

Y. K. Levine
Department of Molecular Biophysics, Buys Ballot Laboratory, University of Utrecht, P.O. Box 80.000, 3508 TA Utrecht, The Netherlands

(Received 20 February 1990)

The clustering process in sodium di(2-ethylhexyl)sulfosuccinate–H_2O–iso-octane microemulsions has been studied by dielectric relaxation spectroscopy and small-angle x-ray scattering (SAXS). The SAXS experiments are interpreted using the pair-correlation function for the microemulsion droplets obtained from the multicomponent sticky hard-sphere-droplet model. The results indicate the presence of a strong interaction between the droplets and the solvent medium. The structural parameters extracted from this analysis are used to calculate the correction term to the Clausius-Mossotti equation for the polarizability of the microemulsion system. Good agreement is found between the observed and calculated polarizabilities.

I. INTRODUCTION

The sodium di(2-ethylhexyl) sulfosuccinate (AOT) molecule is a double-chained ionic surfactant capable of dispersing large amounts of water and oil, two otherwise immiscible liquids. As a result of their amphilic structure the molecules reside at the oil-water interface with the hydrocarbon chains directed toward the oil phase and the ionic head groups solvated in the water, thereby causing a marked reduction in the interfacial tension.[1–4]

A large region of the AOT–H_2O–iso-octane phase diagram consists of the so-called microemulsion phase, which is fluid, transparent, isotropic, and thermodynamically stable at room temperature. In this water-in-oil microemulsion the water is dispersed in the oil medium as small spherical (nanometer-sized) droplets surrounded by a monomolecular layer of surfactant molecules.[5–15] The curvature of the interface toward the water is believed to be dictated by the cone-shaped geometry of the AOT molecules. This is widely regarded as the driving force for the formation of a water-in-oil microemulsion phase in this sytem. The droplet size is determined by the molar water-surfactant ratio, W_0, while the concentration of the droplets is determined by the molar ratio of oil to surfactant, S_0.[10,16,17]

Interestingly, a percolationlike transition in the dielectric behavior has been observed within the microemulsion phase region of the AOT–H_2O–iso-octane system.[18–25] This percolation transition can be induced by raising the concentration of the dispersed water and is characterized by an increase in the conductivity of the microemulsion by at least five orders of magnitude. Simultaneously, the low-frequency permittivity ϵ_{LF} of the system diverges and can exceed values of 100.[18–21] Furthermore, this percolation transition can also be induced by increasing the temperature at constant microemulsion composition.

Our laboratory has previously reported an extensive study of the dielectric properties of the AOT–H_2O–iso-octane system[18–21] and proposed a "macrofluid" model for describing the observed polarizabilities. In this model the microemulsion is taken to consist of interacting droplets and the deviations of the observations from a classical Clausius-Mossotti behavior have been rationalized in terms of the formation of droplet clusters. The divergence of the permittivity is attributed to excess dipole-polarization associated with the contact regions between the droplets.[19,26] The modification to the Clausius-Mossotti relation explicitly contains the pair-correlation function $g(r)$. This function, well known from liquid-state thermodynamics, describes droplet-droplet correlations.[27,28] Unfortunately $g(r)$ cannot be extracted from dielectric relaxation experiments as these only yield information about macroscopic properties.

Nevertheless, the pair-correlation function $g(r)$ can be determined in experiments utilizing scattering of electromagnetic radiation. It is well known that small-angle x-ray scattering (SAXS) experiments can be used to access the Fourier transform of $g(r)$, the structure factor $S(q)$, in colloid-particle systems with particle size between 1 and 100 nm.[29,30] The structural information obtained from SAXS experiments can now be combined with the model describing the dipole polarizability of the microemulsion clusters in order to calculate the modifications to the Clausius-Mossotti relation. In this way the dielectric permittivity of the microemulsion can

be predicted as a function of temperature and composition. To our knowledge such a quantitative comparison between the microscopic structure and macroscopic behavior of these systems has not been attempted as yet.

This approach is impeded by the fact that the pair-correlation function $g(r)$ cannot be obtained in a straightforward manner from the SAXS intensity curves as a consequence of the inherent structural polydispersity of the microemulsion systems.[10,11,17,31,32] Nevertheless, we have recently shown[33] how to express the pair-correlation function for a system of interacting particles with size dispersity within the Percus-Yevick formalism.

This multicomponent model for sticky hard spheres[33] is used in this paper for the analysis of SAXS intensity curves obtained from AOT–H_2O–iso-octane microemulsions at various concentrations and temperatures.

This paper is organized as follows. In Sec. II we outline the model used for describing the dielectric properties of the microemulsion in terms of polarizability of the medium. In Sec. III we consider the consequences of the polydispersity in droplet size, and show that a moderate variation in the droplet size does not have any effect on the permittivity of the medium. In Secs. IV and V we present a detailed analysis of SAXS experiments on two microemulsion systems, with different average droplet sizes $W_0=25$ and 35. In Sec. VI we compare the polarizabilities calculated from the structural parameters obtained from the analysis of the SAXS experiments and those measured in dielectric experiments.

II. PERMITTIVITY IN TERMS OF POLARIZABILITY

The dipole polarizability α_p of a homogeneous sphere of permittivity ϵ_p suspended in a medium permittivity ϵ_0 is given by

$$\alpha_p=\frac{\epsilon_p-\epsilon_0}{\epsilon_p+2\epsilon_0}\ . \tag{1}$$

For a sufficiently dilute dispersion of spheres the Clausius-Mossotii (CM) relation is valid, giving the effective polarizability of the medium as[34]

$$\alpha\equiv\frac{\epsilon-\epsilon_0}{\epsilon+2\epsilon_0}=\alpha_p\phi_p \tag{2}$$

where ϕ_p is the volume fraction occupied by the particles and ϵ is the measured permittivity. The CM relation can be extended to the case of higher volume fraction by considering the contributions to the dipole polarizability arising from all the possible pairs of spheres present in the mixture. It has been previously shown that this correction term can be incorporated in the CM relation in a general operational way as[19]

$$\alpha=\alpha_p\phi_p[1+I_2(\phi_p,T)\phi_p]\ . \tag{3}$$

The correction term $I_2(\phi_p,T)$ describes the fact that at larger volume fractions, when clusters of particles are formed, the polarizability per unit volume increases significantly above the value of a single sphere. The increase in the dipole polarizability due to two-sphere interactions is of the form[19,26]

$$I_2(\phi_p,T)=\frac{4\pi}{V_p}\int_0^\infty dr\, r^2 g(r)\Delta(r) \tag{4}$$

where $g(r)$ is the usual pair correlation function, V_p the volume of a sphere, and $\Delta(r)$ the excess polarizability of a pair of spheres. This is in turn given by

$$\Delta(r)=\frac{\alpha_2(r)-\alpha_p}{\alpha_p} \tag{5}$$

with $\alpha_2(r)$ the polarizability of a pair of spheres separated by distance r and averaged over all orientations. Bedeaux, Wind, and van Dijk[26] have shown furthermore that the excess polarizability $\Delta(r)$ of two conducting spheres, of diameter D, is sharply peaked at the point of contact, $r=D$, and decays rapidly to zero for larger r.[26] We note here that Eq. (4) is exact only in the case whereby the multiplet excess polarizabilities are negligible.

Equation (3) has been shown to be remarkably successful in describing the dielectric permittivity of AOT–H_2O–iso-octane microemulsions.[21] These microemulsions may be considered as a macrofluid of small droplet suspended in a continuous oil phase. Each droplet consists of a water core surrounded by a monomolecular layer of AOT molecules. It was found that α_p at a constant water-surfactant ratio is independent of temperature and volume fraction. Surprisingly however the correction $I_2(\phi_p,T)$ at a given water-surfactant ratio was found to be independent of the volume fraction ϕ_p but exhibited an Arrhenius temperature dependence.[19] As α_p and $\Delta(r)$ only depend on the dielectric structure of the microemulsion particle, it was concluded that the microemulsion droplets do not change shape or size on varying the temperature or microemulsion composition.

The finding that $I_2(\phi_p,T)$ is independent of the volume fraction is remarkable, particularly in view of the fact that it is a function of the pair correlation function $g(r)$, Eq. (4). As in general $g(r)$ depends on the particle concentration, we intuitively expect to observe a volume-fraction dependence for I_2.

In this section we shall consider the possible origin of this behavior and outline a method for obtaining a theoretical expression for $I_2(\phi_p,T)$ based on a realistic microscopic model of the microemulsion structure. To this end we shall need expressions for the pair-correlation function $g(r)$ and the excess dipole polarizability function $\Delta(r)$, appearing in Eq. (4).

A. Model for $\Delta(r)$

The model for the dielectric permittivity behavior of microemulsion systems presented by Bedeaux, Wind, and van Dijk[26] and van Dijk and co-workers[18–21] in terms of a dispersion of conducting spheres in a nonconducting medium is highly idealized. A more realistic model must incorporate the effects of the surfactant molecules adsorbed in the water-oil interface. We shall therefore consider here each microemulsion droplet to consist of a conducting sphere, representing the water core with the surfactant counter ions, surrounded by a nonconducting layer with a permittivity equal to that of the medium. This nonconducting layer represents the apolar part of the sur-

factant solvated in the continuous oil phase. The length of the nonconducting layer will only be equal to that of a surfactant molecule, provided the oil-phase molecules are rigorously excluded from it. However as we cannot rule out a partial penetration of the oil, we expect the length of the nonconducting layer to be somewhat larger than that of a single surfactant molecule.

In the absence of a closed expression for $\Delta(r)$, for this model, we approximated the expression given by Bedeaux, Wind, and van Dijk[26] by the function

$$\Delta(r)=\begin{cases}\frac{1}{2}\left[1+\frac{1}{\omega^2}(r-D_\infty)^2\right]^{-1}+\frac{1}{2}\left[1+\left[\frac{16}{\omega}\right]^2(r-D_\infty)^2\right]^{-1}, & r\geq D_\infty \\ 0, \quad r<D_\infty .\end{cases} \tag{6}$$

This function enables us to reproduce the two principle features of the conducting-sphere model for the microemulsions droplets, namely the sharp peak at $r=D_\infty$ and the long decaying tail. Here D_∞ is the diameter of the conducting sphere and the decay constant ω characterizes the range of the excess polarizability function $\Delta(r)$. We have found that a good approximation of the excess polarizability given by Bedeaux[26] and van Dijk[21] is obtained on taking D_∞/ω equal to 15. The dependence of the excess polarizability function Eq. (6) on D_∞/ω is shown in Fig. 1.

B. Model for $g(r)$

We shall now obtain the pair correlation function $g(r)$ by considering the microemulsion system to be a macrofluid[10,11,15,17] and treat the microemulsion droplets as identical particles dispersed in vacuum. We shall take the interaction potential between two droplets to consist of a hard repulsive core with an additional contribution from an attractive short-range term. This latter contribution is the simplest interaction term necessary for describing the clustering phenomena observed in the microemulsion systems. This sticky hard-sphere potential (SHS) introduced by Baxter[35] is defined by

$$\Phi(r)=\begin{cases}\infty, & r<D' \\ \ln\left[12\tau\frac{(D-D')}{D}\right], & D'<r<D \\ 0, & D<r\end{cases} \tag{7}$$

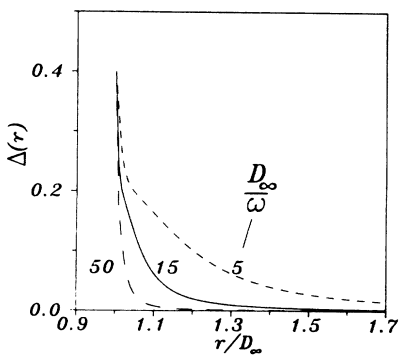

FIG. 1. Model excess polarizability function $\Delta(r)$ [Eq. (6)] for three values of D_∞/ω: 5, 15, and 50.

in the limit $D'\rightarrow D$ with D the diameter of the particles and τ the stickiness parameter determining the measure of attraction. The hard-sphere potential is recovered from Eq. (7) in the limit $\tau\rightarrow\infty$ and the contribution of the surface attraction increases on decreasing the value of τ. We note here that the range $D-D'$ of the attractive term in the SHS potential Eq. (7) is zero for a given value of τ. The solution of the Ornstein-Zernike integral equation for the SHS potential was given by Baxter[35] within the Percus-Yevick (PY) approximation.[36] Interestingly, it has been shown recently that this solution yields a good approximation for the behavior of fluid systems of molecules interacting through an attractive square-well potential.[37,38] In particular, if the range of attraction does not exceed 10% of the molecular diameter the systems are well modeled by the SHS potential, Eq. (7).[39]

The solutions of the PY formalism for the hard-sphere and sticky hard-sphere potentials are not entirely analytic and do not yield closed expressions for $g(r)$. Consequently, efficient numerical algorithms have been developed for the evaluation of the pair correlation function with great precision.[40,41] Our method for the evaluation of $g(r)$ for the SHS potential is summarized in the Appendix and closely follows the approach proposed by Perram[42] and Barker and Henderson[40,43] in obtaining $g(r)$ for the case of the hard-sphere fluid. However, some care has to be taken in our SHS case as the correlation functions and their derivatives have discontinuities at $r=D$, $2D$, $3D$, etc. The solution for $g(r)$ is found to be:

$$xg(x)=\begin{cases}\frac{\lambda}{12}\delta(x-1^-), & 0<x<1 \\ a_1e^{\mu x}+e^{\eta x}[a_2\cos(\xi x)+a_3\sin(\xi x)], & 1<x<2\end{cases} \tag{8}$$

where a_1, a_2, a_3, λ, μ, η, and ξ (see Appendix) are functions of ϕ and τ, x is the reduced distance r/D, and 1^- denotes the left-hand limit. The solution for $g(x)$ in the intervals $2<x<3$, $3<x<4$, etc., can be simply obtained by the successive application of the propagator equation, Eq. (A7) of the Appendix. We note here that as $g(x)$ and its derivatives are well behaved (piecewise continuous) for $x>2$, the efficient algorithm proposed by Glandt and Kofke[44] can be used in the numerical computations. Now, successive applications of the trapezoidal rule yield the numerical values of $g(x)$ to any required accuracy.

However, here we shall only be concerned with the ex-

pression for $g(x)$ in the range $0<x<2$, as the excess polarizability $\Delta(r)$ does not differ significantly from zero for $x>2$.

C. $I_2(\phi,T)$ for the SHS model

In order to gain insight into both the effect of the surface adhesion term of the interaction potential on the dielectric polarizability as well as its volume-fraction dependence, we shall consider the case where the excess polarizability of a pair of conducting spheres is represented by a δ function at $x=1$. For this case the correction term of the polarizability I_2, Eq. (4), is given by

$$I_2(\phi,T)=\frac{4\pi}{V_p}\int_0^\infty dr\, r^2 g(r) D\delta(r-D)$$

$$=\frac{4\pi D^3}{V_p}\frac{1}{2}[g(D^-)+g(D^+)]=\tfrac{1}{2}\lambda(1+\tau)\,, \qquad (9)$$

It is important to note now that λ is a function of both ϕ and τ (see Appendix). Consequently we also expect I_2 to exhibit a dependence on the volume fraction ϕ. Equation (9) shows that I_2 is defined by both the right- and left-hand limit of $g(r)$ at $r=D$. The value of the left-hand limit $g(D^-)$ is directly proportional to the number of bound spheres (particles) in the system. However, the right-hand limit $g(D^+)$ represents the contribution to I_2 from those spheres that are close, yet not in contact with each other. It is clear that the contribution from $g(D^-)$ to I_2 becomes dominant on increasing the stickiness of the particles, while the term $g(D^+)$ becomes important on decreasing the stickiness. For a repulsive hard-core potential this term is a slowly increasing function of the volume fraction.

Figure 2 shows the dependence of I_2 on the volume fraction of the spheres ϕ for different values of the stickiness (surface adhesion) parameter τ. I_2 can be seen to decrease with decreasing stickiness (increasing τ) at every volume fraction ϕ. The volume-fraction dependence of I_2 is rather difficult to understand physically. It appears to be determined by the relative contributions of $g(D^-)$ and $g(D^+)$ at a given value of the stickiness parameter.

The results shown in Fig. 2 can now be used to rationalize the experimental observation that I_2 is independent of the volume fraction ϕ. This behavior implies [Eq. (9)],

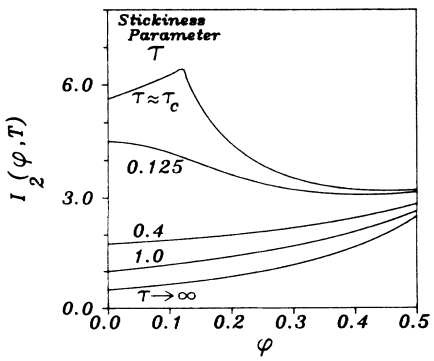

FIG. 2. Volume-fraction dependence of I_2 for the sticky hard-sphere system at five values of the stickiness parameter τ. $\tau\to\infty$ corresponds to hard spheres with no attraction.

that the stickiness must vary with the volume fraction so as to cancel the ϕ dependence in λ. As in the SHS model I_2 is found to decrease with decreasing stickiness, we conclude that the stickiness must decrease with increasing volume fraction in order to make I_2 independent of the volume fraction. We shall see that this is an important prediction.

We shall now consider qualitatively the effect of the finite range of the excess dipole polarizability $\alpha_2(r)$ on I_2. In addition we shall also take into account a difference between the hard-sphere diameter $D_{\rm HS}$ of a particle and the diameter of the water core D_∞ such that $D_{\rm HS}>D_\infty$. This difference may be viewed as the contribution of the nonconducting surfactant layer to the size of a microemulsion droplet. It is clear that a larger range of $\alpha_2(r)$, corresponding to a larger value of ω in Eq. (6), will result in an increase in the value of I_2 at a fixed volume fraction and stickiness. This increase arises from the fact that particles that are close to each other, but not in direct contact, contribute to I_2. On the other hand, an increase in $D_{\rm HS}$ at a constant value of D_∞ will have the opposite effect, and cause I_2 to decrease. We thus conclude that the dependence of I_2 on the volume fraction may be eliminated if the hard-sphere diameter $D_{\rm HS}$ exhibits a dependence on ϕ.

The experimental observation from dielectric measurements[19] that I_2 is independent of ϕ can thus be explained in terms of two distinct physical effects: a ϕ dependence of the stickiness and a volume-fraction-dependent hard-sphere diameter. In order to be able to distinguish between these effects, we have incorporated both ϕ dependencies in our model. This is justified by the fact that SAXS experiments monitor both the diameter of the water core and the contribution of the surfactant layer to the hard-sphere diameter and in addition yield the stickiness parameter.

III. POLYDISPERSITY

Colloidal systems exhibit various kinds of polydispersity on a microscopic level.[17,31,32] For example, the polydispersity in the particle diameter of a microemulsion arises from the competition between opposing contributions to the free energy such as surface tension, electric double-layer potential, and surfactant interactions. This property impedes the interpretation of experiments monitoring the microscopic properties of the system. It thus becomes necessary to incorporate polydispersity explicitly in the analysis of SAXS experiments. This can only be done using reasonable models for the size distribution functions. We now note that any unimodal distribution function may in practice be represented by a Gaussian or generalized exponential distribution to a good approximation.

We shall restrict our discussion to systems exhibiting polydispersity in size and interaction potentials, both of which can be treated within the framework of the Percus-Yevick formalism.[45–48] The microemulsion particles will be considered to be spherical, so that the size distribution simply describes the differences in the particle diameters. Furthermore, we shall take the attractive

term in the interaction potential to be different for particles of different size.

It has been shown previously that both types of polydispersity can be incorporated explicitly into the PY formalism provided the distribution functions are expressed in discrete forms.[33,45–48] In this case, the equations are transformed to matrix equations from which the pair-correlation functions can be evaluated numerically. In practice, however, it may not be feasible to distinguish between dispersion in interaction and a dispersion in size, as their effects on the properties monitored in an experiment will almost always be correlated. Thus, unless one of the polydispersities is small, it will be difficult to estimate accurately the distribution function of the other. The correction term I_2 of the effective polarizability considered above involves to a first approximation only the value of the pair-correlation function at the point of contact, or in other words, the number of contacts between the spheres in the system.[26] As this quantity can be calculated analytically for the multicomponent SHS system, we shall use it here to illustrate the effects of both types of polydispersities on the total effective polarizability.

First, we shall consider the effect of polydispertiy in particle size on the average number of bonds per particle z in a multicomponent SHS system. In order to do this we define a system containing p classes of spherically symmetric particles with number densities x_n, $n=1,\ldots,p$, differing in their hard-sphere diameters D_n. The number density x_n of particles in class n is given by the discrete form of the Schulz size distribution. This distribution[49] has proved to be particularly useful for modeling the size polydispersity and was used by us previously for the analysis of SAXS experiments.[33,50–56]

The average number of bonds per particle (coordination number) z is defined by

$$\frac{N}{V}z=\frac{1}{2}\sum_{n=1}^{p}x_n P_{n,\text{pair}} , \tag{10}$$

where $P_{n,\text{pair}}$ is the probability that a particle is bound to a particle in class n, and N/V is the average number of particles per unit volume. $P_{n,\text{pair}}$ may be expressed in the probability P_{nm} which is the probability that a particle of class m is bound to a particle of class n:

$$P_{n,\text{pair}}=\sum_{m=1}^{p}x_m P_{nm} . \tag{11}$$

P_{nm} can be expressed in terms of the usual multicomponent pair-correlation functions $g_{nm}(r)$:

$$P_{nm}=\int_0^{1/2(D_n+D_m)} dr\, 4\pi r^2 g_{nm}(r)=\frac{\pi}{24}\lambda_{nm}(D_n+D_m)^3 . \tag{12}$$

Here $g_{nm}(r)$ and λ_{nm} are obtained from the polydisperse equivalent of Eq. (8) for $g(x)$, $x=r/D$, and Eq. (A2) for λ appearing in the PY formalism for the interaction potential between particles of classes m and n:[45]

$$\Phi_{nm}(r)=\begin{cases}\infty, & 2r<s_{nm}\\ \ln\left[12\tau_{nm}\dfrac{D_n+D_m-s_{nm}}{D_n+D_m}\right], & s_{nm}<2r<D_n+D_m\\ 0, & D_n+D_m<2r\end{cases} \tag{13}$$

with $s_{nm}\to D_n+D_m$ and with all the parameters τ_{nm} equal, corresponding to a monodisperse interaction. Note that we define the interaction to be polydisperse when the parameters τ_{nm} describing the stickiness between particles of classes m and n are different. The numerical solution of the PY equations for this potential has been described by us previously.[33] Using Eqs. (10)–(12) we find

$$\frac{N}{V}z=\frac{\pi}{48}\sum_{n,m=1}^{p}x_n x_m\lambda_{nm}(D_n+D_m)^3 . \tag{14}$$

It is important to note that in the derivation of Eq. (14) we have effectively neglected the contributions to $g(r)$ from the region $1<r/D<2$ [Eq. (8)]. Furthermore, for the monodisperse case λ is given by Eq. (A2) in the appendix.

The dependence of the coordination number z on the particle volume fraction ϕ at different relative dispersions in particle size is shown in Fig. 3. The main effect of introducing polydispersity in the particle size appears to be a decrease in the number of contact points z. This effect is relatively large for low stickiness (high τ) and becomes relatively less important when the stickiness increases (low τ). Furthermore, the relative change in z increases with increasing volume fraction. Overall, however, the effect of the polydispersity in size on z is limited and does

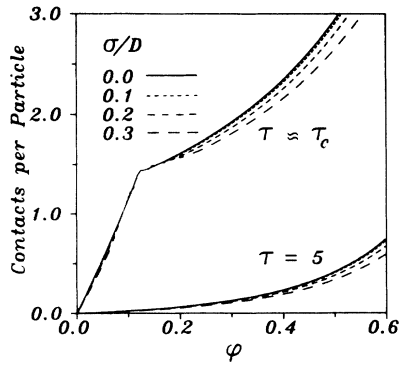

FIG. 3. Average number of contacts per particle z vs the volume fraction ϕ, for two sticky hard-sphere dispersions with $\tau=5$ and 0.0975 ($\approx\tau_c$) with no polydispersity (solid line) and with relative polydispersities $\sigma/D=0.1$ (dotted line), 0.2 (short-dashed line), and 0.3 (long-dashed line).

not exceed 10%. We may therefore safely assume the effect of the size distribution on the effective polarizability of a dispersion of spheres to be negligible.

In contrast to the effects of size distribution considered above, it is difficult to obtain a quantitative estimate of the effect of a dispersion in interaction on the coordination number z of a dispersion of spheres. The reason for this difficulty is that we have no *a priori* model for the distribution of the stickiness matrix elements τ_{nn} entering the potential [Eq. (13)]. Nevertheless an analysis of this effect may be attempted using our previous observations[33] that the average stickiness in the microemulsion system depends on the average size of the particles. It was found that for a monodisperse interaction potential the apparent stickiness between larger particles was systematically less than the stickiness between smaller particles. The relative difference however was found to be smaller than a factor of 10. We have therefore considered the case for which the diagonal matrix elements of the stickiness matrix, describing the stickiness of two spheres of the same size class, vary linearly by an order of magnitude between the two extreme populations with diameters $D+3\sigma$ and $D-3\sigma$. The nondiagonal elements, describing the stickiness between spheres of two different diameters, were taken as the average of the two corresponding diagonal elements. On the basis of these considerations we estimate z will increase by not more than 30%.

We conclude this section by noting that in general a size dispersion decreases the coordination number of a system of sticky spheres, while a dispersion in stickiness has a compensating effect by increasing the coordination number. If the distribution functions describing these dispersions are not too wide the effects are small. Furthermore, because the size and interaction dispersions have opposite effects on the coordination number we may assume that neglecting both types of dispersion will not cause too great an error in the calculation of I_2.

The procedures described above can also be used to show that the effects of both types of polydispersity on SAXS intensity curves are correlated in a way similar to that calculated above for z. Thus the polydispersity in the size compensates the polydispersity in stickiness to a large extent. We have consequently analyzed the SAXS observations using a single stickiness parameter, but a distribution in the microemulsion particle size.

IV. SAXS EXPERIMENTS

The average intensity of scattered radiation from a system of p different types of particles, each with number density x_n is given by[30,53]

$$\frac{I(q)}{V}=I_e\sum_{n,m=1}^{p}(x_nx_m)^{1/2}F_n(q)F_m(q)S_{nm}(q)\ ,$$
$$S_{nm}(q)=(x_nx_m)^{1/2}V^{-1}\left\langle\sum_{n,m=1}^{p}e^{i\mathbf{q}\cdot(\mathbf{R}_n-\mathbf{R}_m)}\right\rangle \tag{15}$$
$$=\delta_{nm}+(x_nx_m)^{1/2}\int_V[g_{nm}(\mathbf{r})-1]e^{i\mathbf{q}\cdot\mathbf{r}}d^3\mathbf{r}\ ,$$

where $q=4\pi/\lambda_e\sin(\theta/2)$ with θ the angle at which the scattered radiation of wavelength λ_e is observed. I_e is a constant factor depending on the experimental setup. It can be taken to be unity as in general we are not concerned with absolute values of the scattered intensity. $F_m(q)$ is the amplitude scattered by the mth particle located at $\mathbf{R}_m$ relative to an arbitrary origin and is given by

$$F_m(q)=\int_V\rho_m(r)e^{i\mathbf{q}\cdot\mathbf{r}}d^3\mathbf{r} \tag{16}$$

with $\rho_m(r)$ the electron density of the mth particle. The integral extends over the scattering volume. We have assume here that the particles have a centrosymmetric electron-density profile. The pair-correlation functions $g_{nm}(r)$ defined above are related by Fourier transformation to the static structure factors $S_{nm}(q)$. It is clear from Eq. (15) that only the Fourier transforms of the pair-correlation functions $g_{nm}(r)$ are experimentally accessible. Furthermore, the scattered intensity of a multicomponent system is given by an average over a matrix of structure factors each weighed by the form factors $F_n(q)$. This in fact creates the major obstacle in the analysis of scattering data. The evaluation of Eq. (15) has been described by us previously.[33]

For a given microemulsion droplet size and droplet concentration, defined respectively by W_0 (water-surfactant concentration ratio) and S_0 (oil-surfactant concentration ratio), the SAXS intensity is described by the electron-density profile of the droplet $\rho_e(r)$ and the pair-correlation function $g(r)$. The latter quantity is obtained from the PY formalism using the SHS model as described above. The electron-density profile for a single droplet used here is based on the chemical structure of the AOT molecules and essentially consists of a positive electron-density core relative to the surrounding oil medium. This core, corresponding to the water droplet, is surrounded by a shell of the electron-rich headgroups; see Fig. 4. The surfactant layer, with the AOT hydrocarbon tails dissolved in the oil medium, has the same electron density as the solvent medium and therefore does not contribute to the scattered intensity of a single particle. Consequently six parameters enter the calculation of the scattered intensities:

(1) average diameter of the water core, D_w ;

(2) diameter of the AOT head group, l_h ;

(3) electron density of the head group, ρ_h ;

(4) apparent length of the surfactant layer, l_t ;

(5) variance of the diameter size distribution, σ ;

(6) average (apparent) stickiness parameter, τ .

The hard-sphere interaction diameter is distributed according to the Schulz size distribution with mean value $D_{\mathrm{HS}}=D_w+2l_h+2l_t$ and variance σ. We note that the contribution of the surfactant layer l_t to the hard-sphere diameter has been taken as an adjustable parameter. This allows us to take into account an overlap (interdigitation) of the AOT surfactant tails or an oil penetration into the

surfactant layer. We note furthermore that the parameters l_n and ρ_h unfortunately cannot be determined uniquely from the experimental data as to a first approximation only their product enters the calculations of the scattering curve. However, we have previously shown[57] from an analysis of the high-angle region of the scattering, that we can take ρ_h to be a constant with a value of 850 electrons per nm^3. In order to analyze the SAXS curves we have minimized the difference between measured and calculated intensities from the multicomponent SHS model using nonlinear least-squares fits using the Levenberg-Marquardt[58] algorithm. The question now arises as to the correct choice of the weighting of the residues of the experimental data. Unfortunately, the exact calculation of the errors propagated during the manipulations of the scattered intensity is too cumbersome. We have therefore analyzed the experiments weighting the residues with the square root of the observed intensities. Ideally the results of the analysis should be independent of the choice of weights.

It turns out that the only parameters sensitive to the choice of weights are τ and l_t. On weighting the residues with the intensity we found small systematic errors in the fits at the low-angle regions of the scattering curves and these were particularly noticeable at microemulsion concentrations greater than 30%. On the other hand, when weighting with the square root of the intensity, small systematic errors only occur at the high-angle portion of the curves over the entire concentration range studied. The errors found in the high-angle regime are due to the incomplete description of the electron density profile of the particle, while the deviations in the low-angle portion arise from an inaccurate description of the structure factor $S(q)$. As we are primarily interested in the interactions between the particles, we have used the latter weighting in the fitting procedures.

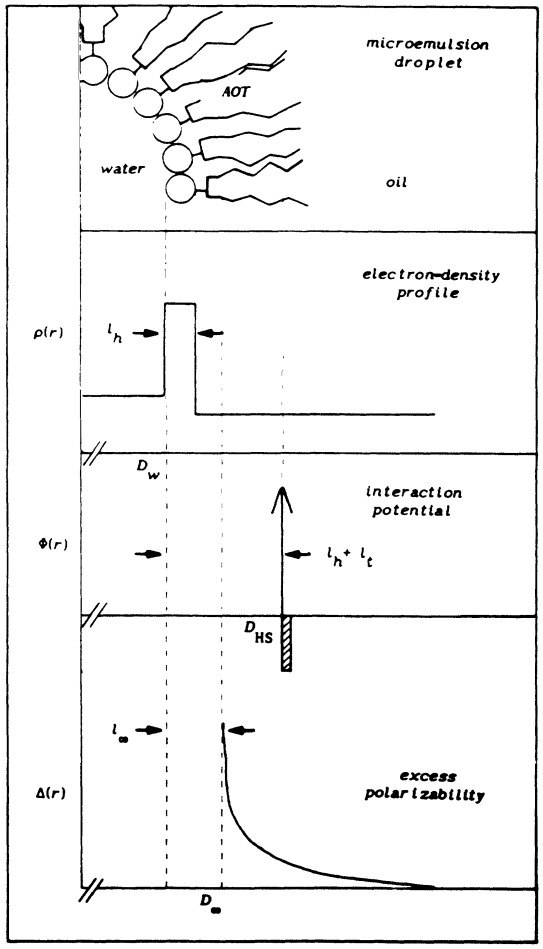

FIG. 4. Model functions representing a microemulsion droplet. Electron-density profile $\rho_e(r)$, sticky hard-sphere potential $\Phi(r)$, and excess polarizability function $\Delta(r)$.

A. Relation between particle, hard-sphere, and water volume fractions

In the foregoing discussion we introduced four different quantities for describing the size microemulsion droplets or particles:

(1) water droplets, diameter D_w;

(2) microemulsion droplets, diameter D_p;

(3) hard spheres, diameter D_{HS};

(4) conducting spheres, diameter D_∞.

In this section we shall consider unambiguous definitions for the corresponding volume fractions.

The volume fraction of water ϕ_W, which can be calculated using the known densities bulk densities of water, AOT,[59] and solvent is given by

$$\phi_w = \frac{M_w \rho_w^{-1} W_0}{M_w \rho_w^{-1} W_0 + M_s \rho_s^{-1} + M_0 \rho_0^{-1} S_0} , \tag{17}$$

where ρ_w, ρ_s, and ρ_0 are the densities of water, AOT, and solvent and M_w, M_s, and M_0 are the molecular weights of water, AOT, and solvent, respectively. W_0 and S_0 are determined by the known weighed amounts of water, AOT, and solvent.

On assuming a microemulsion droplet to consist of only water and AOT we may write analogously for the volume fraction of microemulsion droplets ϕ_p

$$\begin{aligned}\phi_p &= \frac{M_w \rho_w^{-1} W_0 + M_s \rho_s^{-1}}{M_w \rho_w^{-1} W_0 + M_s \rho_s^{-1} + M_0 \rho_0^{-1} S_0} \\ &= \phi_w \left[1 + \frac{M_s \rho_s^{-1}}{M_w \rho_w^{-1} W_0} \right] .\end{aligned} \tag{18}$$

The microemulsion droplets are not all identical but show a dispersion in size. This polydispersity is conveniently described with the discrete form of the Schulz size distribution. The volume fraction of water [Eq. (17)] and the volume fraction of particles [Eq. (18)] are now simply expressed as

$$\phi_w = \frac{\pi}{6} \frac{N}{V} \langle D_w^3 \rangle , \quad \phi_p = \frac{\pi}{6} \frac{N}{V} \langle D_p^3 \rangle , \tag{19}$$

where $\langle\ \rangle$ denotes averages over the size distribution. As D_w is directly monitored in the SAXS experiment, we are

now able to determine the number density N/V of the microemulsion droplets by combining Eqs. (17) and (19). Equations (18) and (19) can be seen as the definition of the microemulsion particle diameter D_p. The knowledge of N/V together with the determination of D_{HS} from the SAXS curves allows us to calculate the hard-sphere volume fraction ϕ_{HS} from

$$\phi_{HS}=\phi_w \frac{\langle D_{HS}^3 \rangle}{\langle D_w^3 \rangle} . \tag{20}$$

The difference between D_{HS} and D_w represents the size of the surfactant layer relative to the hard-sphere diameter and will henceforth be denoted as [see Fig. 4]:

$$D_{HS}-D_w=2l_{HS}=2(l_h+l_t) .$$

In the calculation of the polarizability and the volume fraction of conducting spheres ϕ_∞ we denote the difference between D_∞ and D_w by $2l_\infty$, and use the definition

$$\phi_\infty=\phi_w \frac{\langle D_\infty^3 \rangle}{\langle D_w^3 \rangle} , \tag{21}$$

l_∞ represents the contribution of the polar part of the AOT molecule to the conducting sphere and has been taken to be 0.6 nm in accordance with molecular models of the molecule, see Fig. 4.

The area per surfactant molecule at the water interface is simply given by

$$\Sigma_s=6W_0 v_w \frac{\langle D_w^2 \rangle}{\langle D_w^3 \rangle} , \tag{22}$$

where v_w ($=0.03$ nm^3) is the volume of a H_2O molecule. Σ_s plays an important role in the theory of micelle and microemulsion formation.[1,2,17,29] Equation (22) has been derived on assuming that all the AOT molecules are absorbed at the water-oil interface. This assumption is justified as the AOT concentrations used in our experiments exceed the critical micelle concentration by at least an order of magnitude.[3,4]

B. Materials and methods

The surfactant Aerosol-OT [AOT, sodium di(2-ethylhexyl) sulfosuccinate] was obtained from Fluka Chemie AG, purity >98%, and was purified according to Tavenier.[60] Iso-octane (2,2,4-trimethyl pentane), *n*-hexane, and *n*-heptane were purchased from Merck and *n*-decane was obtained from Fluka Chemie AG. All organic solvents were analytic grade and used without further purification. The water used was deionized and quadruple distilled in a quartz still.

For each solvent a concentration series of samples with constant water-surfactant ratio W_0 ($\cong 25$) and increasing S_0 was prepared. In a single series a stock microemulsion solution with the lowest S_0 was prepared by dissolving a weighed quantity of AOT in the appropriate amount of solvent. Water was then added to establish the desired value of W_0. The S_0 values were increased by dilution of the stock solution. The samples were allowed to equilibriate at room temperature for more than 24 hours before the experiments. All the samples remained stable and optically clear over a period of months. Furthermore, no sample degradation was observed during the exposure to the x-ray beam and the results obtained were independent of the history of the sample.

The small-angle x-ray scattering experiments were performed at Daresbury Laboratory, United Kingdom, using station 8.2 of the SRS with a setup as described in Ref. 57. Dielectric relaxation experiments were performed using a Hewlett-Packard HP4192A impedance analyzer in the frequency range 10 kHz to 13 MHz. Measurements in the 5- to 1000-MHz range were carried out with a Rohde & Schwarz ZPV vector voltmeter equipped with a ZPV-E2 tuner unit. The sample cell was similar to that described in Ref. 21.

The complex permittivity $\epsilon(\omega)$ is expressed as

$$\epsilon(\omega)=\epsilon'(\omega)-i\left[\epsilon''(\omega)+\frac{\kappa}{\omega\epsilon_v}\right] , \tag{23}$$

where ω is the radial frequency, κ the dc conductivity, and ϵ_v the absolute vacuum permittivity ($\epsilon_v=8.854\times10^{-12}$ F m^{-1}). All other permittivities reported here are relative permittivities. Within our experimental frequency range we always observed a frequency-independent portion of the real part of the permittivity at low frequencies. This value will be referred to henceforth as the low-frequency permittivity of the microemulsion. The dc conductivity κ was determined from the measured ω^{-1} dependence of the imaginary part of the permittivity at low frequencies ($\omega<500$ kHz). We note here that the dielectric behavior is described by a complex permittivity $\epsilon(\omega)$ [Eq. (23)] with real $\epsilon'(\omega)$, $\epsilon''(\omega)$, and κ.

For the calculation of the volume fractions of solvent, water, and AOT the following bulk densities were used: water (0.998 g cm^{-3}), iso-octane (0.692 g cm^{-3}), *n*-decane (0.73 g cm^{-3}), *n*-heptane (0.690 g cm^{-3}), and *n*-hexane (0.66 g cm^{-3}). The density for AOT in solution was taken as 1.138 g cm^{-3}.[59]

V. SAXS RESULTS

Typical scattering curves obtained from microemulsions at a constant W_0 (i.e., constant droplet size), are shown in Fig. 5 for oil-surfactant ratios S_0 varying from 5 to 500. The absence of any modulations in the scattered intensity at these angles is a strong indication of a polydispersity in the particle size. The superposition of scattering curves from particles of different sizes, each with a characteristic modulation, results in a smooth decay of the observed intensity curve. The continuous lines in Fig. 5 represent the best fits using the SHS multicomponent model [Eq. (15)]. The broad peak at $q<1$ nm^{-1} typical of microemulsion scattering which appears at high water concentration arises from interference effects. It is well described by the structure factors calculated from the polydisperse macrofluid model.

The average diameter of the water core of the microemulsion particle D_w obtained from the analysis of the

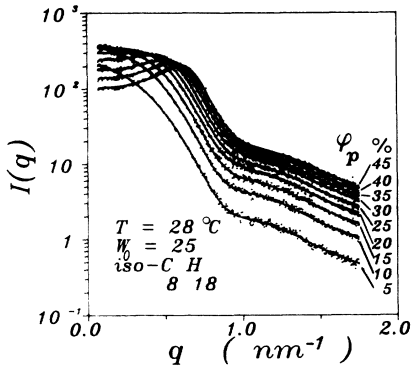

FIG. 5. SAXS intensities from an AOT–H_2O–iso-octane microemulsion concentration series with $W_0=25$ at $T=25$ °C. Line through datapoints represents best fit.

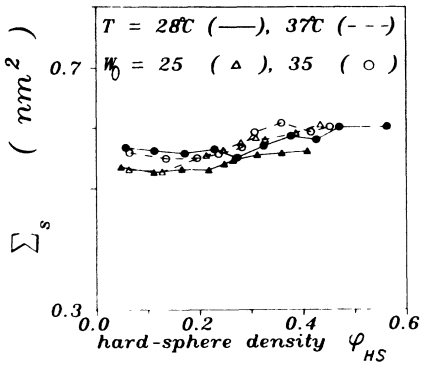

FIG. 7. Area per surfactant molecule Σ_s, see caption of Fig. 6.

scattering curves is shown in Fig. 6 as a function of the hard-sphere volume fraction for two microemulsions with $W_0=25$ and 35 at two different temperatures. It appears that the average size of the water core in both microemulsion systems is virtually independent of the composition and temperature of the system within experimental error. This finding is in good agreement with the observation that the single particle polarizability α_p is independent of temperature and volume fraction.[19]

The average area per surfactant molecule Σ_s calculated from Eq. (22) for these systems is shown in Fig. 7. It can be seen that Σ_s increases slightly, by less than 10%, over the range of volume fractions studied as well as on increasing W_0 from 25 to 35. This is consistent with the modified Porod behavior reported by us previously[57] from the analysis of the high-angle portions of the curves only. A somewhat smaller increase is observed on increasing the temperature at a constant W_0. It is important to note here that the changes in Σ_s described above result from subtle changes in the polydispersity and average particle size in the microemulsion. This may be caused by an increase in mobility of the surfactant tails at higher temperatures inducing a less dense packing of surfactant molecules in the interface or a change in the curvature of the interface itself.

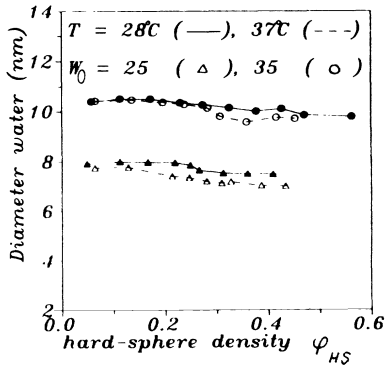

FIG. 6. Diameter of the water core D_w vs hard-sphere density ϕ_{HS} of the AOT–H_2O–iso-octane microemulsion with $W_0=25$ (triangle) and $W_0=35$ (circle) at $T=28$ °C (solid symbols) and $T=37$ °C (open symbols).

The contribution to the hard-sphere diameter l_{HS} and the apparent stickiness parameter τ are given in Figs. 8 and 9, respectively, as a function of the hard sphere volume fraction for two microemulsion systems at different temperatures. For clarity we have shifted the plots in Fig. 9 of the $W_0=25$ microemulsion one order of magnitude.

A systematic increase in the stickiness is observed on increasing the temperature at volume fractions below 0.3. This corresponds to an increase in the clustering of the droplets at higher temperatures, in accord with dielectric permittivity measurements.[19] The formation of large clusters of droplets on increasing the temperature is surprising. Interestingly, only a hard-sphere interaction potential is needed for the description of the SAXS curves obtained at volume fractions greater than 0.3.

The variation of l_{HS} between 1.5 nm at low ϕ and 0.6 nm at high ϕ indicates that oil is absorbed at the surfactant layer at the lower particle concentrations. Consequently as the volume fraction increases with a concomitant decrease in the distance of separation between the microemulsion droplets, the oil is expelled from the surfactant layer. The limiting value of 0.6 nm at high ϕ is about 0.15 nm smaller than the length of the tails of the AOT molecules calculated from their density, 1.14 g cm^{-3}. This calculation assumes an area per surfactant

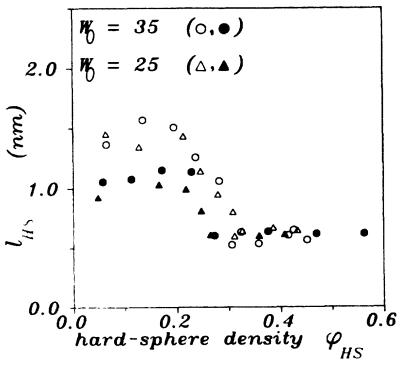

FIG. 8. Contribution (l_t+l_h) to the hard-sphere diameter of the surfactant layer of the AOT–H_2O–iso-octane microemulsion with $W_0=25$ (triangle) and $W_0=35$ (circle) at $T=28$ °C (solid symbols) and $T=37$ °C (open symbols).

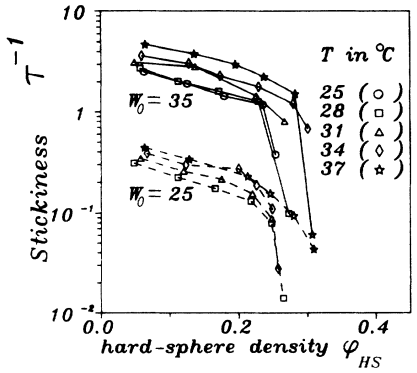

FIG. 9. Stickiness vs hard-sphere density in AOT–H_2O–iso-octane systems with $W_0=25$ and $W_0=35$ at temperatures between 25 °C and 37 °C.

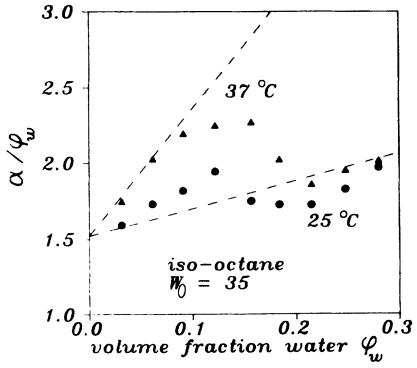

FIG. 10. Calculated (solid symbols) and measured (dashed line) (Ref. 19) polarizabilities α/ϕ_w vs the volume fraction water ϕ_w of the AOT–H_2O–iso-octane microemulsion with $W_0=35$ at $T=25$ °C (circle) and $T=37$ °C (triangle).

molecule of 0.55 nm^2. We therefore expect the surfactant tails of different particles to interdigitate at the highest concentrations.

The observed effects of the oil medium on the microemulsion droplet interaction is not included in the SHS model which implicitly assumes that the droplets are dispersed in vacuum. As the solvent appears to play a role in the clustering of the droplets, we expect the microemulsion properties to be influenced substantially by solvents of different chemical structures. This point will be treated in detail elsewhere.

The decrease of the apparent stickiness with increasing volume fraction ϕ, follows closely that of l_{HS} [Figs. 8 and 9]. We believe that this correlation arises from the nature of the SAXS experiments. It has been shown[39] that the structure factor in SAXS experiments is mainly determined by the second virial coefficient of the equation of state of the fluid system. For the SHS fluid this coefficient is a function of both the hard-sphere diameter and the stickiness parameter τ. We therefore cannot rule out that separate ϕ dependence of τ and l_{HS} in our analysis arises from a deficiency in the description of the actual functional dependence of the second virial coefficient on τ and on l_{HS}.

VI. CALCULATION OF THE POLARIZABILITY

We have noted in Sec. I that the most remarkable finding from the dielectric experiments is that I_2 is independent of the volume fraction of the dispersed particles. We have argued that this behavior can be rationalized by assuming a decrease of the stickiness parameter τ with ϕ. This prediction is indeed in good agreement with the observed ϕ dependence of the stickiness parameter obtained from the analysis of the SAXS intensity curves [Fig. 9]. Moreover the increase of the stickiness with temperature also accounts for the observation that I_2 is an increasing function of T.

Interestingly, we find that the apparent stickiness in the $W_0=25$ microemulsion is systematically higher at temperatures below 31 °C than that for the system with $W_0=35$. The trend, however, is reversed at higher temperatures. This is again in qualitative agreement with the results of dielectric relaxation experiments which show that below 34 °C, $I_2(\phi,T)$ for the $W_0=25$ microemulsion is larger than that for the $W_0=35$ systems, while the opposite is true at higher temperatures.

The dielectric polarizability α of the microemulsion system can be calculated from Eq. (3) using the structural parameters extracted from the analysis of the SAXS intensity curve. In particular, four quantities enter the calculation: (1) the average diameter of the water core D_w, (2) the total length of the surfactant layer contributing to the hard-sphere diameter $2(l_h+l_t)$, (3) the apparent stickiness parameter τ and (4) the volume fraction of the dispersed particles ϕ_w.

The calculated α are shown in Figs. 10 and 11 as a plot of α/ϕ_w versus ϕ_w at two different temperatures for the $W_0=35$ and $W_0=25$ microemulsion, respectively. In Fig. 10 we have taken the experimental data from Ref. 19 for the same system.

As can be seen from Figs. 10 and 11 a reasonable agreement is found between the calculated polarizabilities and the experimental permittivity data at low volume fractions. The calculations also reproduce the observed increase in the polarizability on raising the temperature. However, the calculations underestimate the polarizabilities at high volume fractions. We do not believe that the

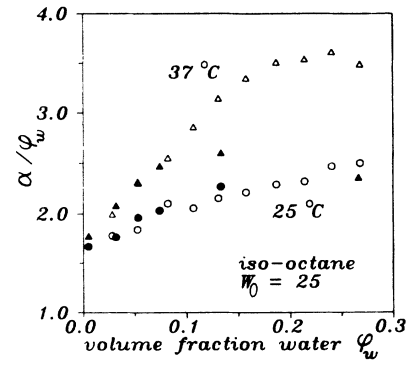

FIG. 11. Calculated (solid symbols) and measured (open symbols) polarizabilities α/ϕ_w vs the volume fraction water ϕ_w of the AOT–H_2O–iso-octane microemulsion with $W_0=25$ at $T=25$ °C (circle) and $T=37$ °C (triangle).

discrepancies found between the experimental and calculated values are caused by the choice of the SHS model in the analysis of the SAXS experiments. Rather, we attribute this disagreement to the simplified model for the excess polarizability, Eqs. (3), (4), and (6). It must be realized that this equation was derived by taking into account only the pair excess polarizabilities. The breakdown may therefore be caused by the neglect of the multiplet excess polarizabilities arising from clusters involving more than two droplets.

ACKNOWLEDGMENTS

The use of the SRS was made possible by the Netherlands Organization for Scientific Research (NWO) in cooperation with the United Kingdom Science and Engineering Research Council (SERC). Special thanks go to members of the SAXS project team at Daresbury Laboratories and Dr. R. E. van Faassen at Utrecht University.

APPENDIX: THE STICKY HARD-SPHERE PAIR-CORRELATION FUNCTION

Baxter[35,45] developed a method to solve the PY equation for a system of identical spheres interacting through the so-called sticky hard-sphere potential [Eq. (7)]. Due to Baxter's factorization, the correlation functions $h(r)$ and $c(r)$ can be expressed in terms of a new function $q(r)$ given by[35,45–48]

$$q(x)=\frac{a}{2}(x^2-1)+b(x-1)+c \quad \text{for } 0<x<1 \tag{A1}$$

with

$$a=\frac{1+2\phi}{(1-\phi)^2}-\frac{\lambda\phi}{(1-\phi)},\quad 2b=\frac{-3\phi}{(1-\phi)^2}+\frac{\lambda\phi}{(1-\phi)},$$
$$c=\lambda/12 .$$

x is the reduced distance r/D, ϕ is the volume fraction of dispersed particles. λ is the solution of the quadratic equation

$$\frac{\phi}{12}\lambda^2-\left[\frac{\phi}{(1-\phi)}+\tau\right]\lambda+\frac{1+2\phi}{(1-\phi)^2}=0 . \tag{A2}$$

In terms of this function the Ornstein-Zernike relation for $c(x)$ and $h(x)$ is given by

$$xc(x)=-q'(x)+12\phi\int_0^1 dt\, q'(x-t)q(t) , \tag{A3}$$

$$xh(x)=-q'(x)+12\phi\int_0^1 dt\,(x-t)h(|x-t|)q(t) , \tag{A4}$$

$$h(x)=-1+\frac{\lambda}{12}\delta(x-1^-) \quad \text{for } x<1 . \tag{A5}$$

To obtain an explicit expression for $h(x)$ at values $1<x<2$ the integration range of Eq. (A4) is divided into three parts. To simplify the equations we define the function $Z(x)=xh(x)$, and change to the integrating variable $y=r-t$. ϵ is taken to be arbitrarily small;

$$\begin{aligned}Z(x)=&12\phi\int_{x-1}^{1-\epsilon}dy\, q(x-y)Z(y)\\&+12\phi\int_{1-\epsilon}^{1+\epsilon}dy\, q(x-y)Z(y)\\&+12\phi\int_{1+\epsilon}^{x}dy\, q(x-y)Z(y) .\end{aligned} \tag{A6}$$

Of these three integrals the first two can be evaluated in a straightforward manner as the integrand is known and result in a polynomial in the fourth degree in x so that

$$Z(x)=P(x)+12\phi\int_{1+\epsilon}^{x}dy\, q(x-y)Z(y) \tag{A7}$$

with

$$\begin{aligned}\phi^{-1}P(x)=&\frac{a}{2}(x^4-12x^2+16x)+b(2x^3-6x^2+8)\\&+6c(x^2-2x)+\lambda\left[\frac{a}{2}(x^2-2x)\right.\\&\left.+b(x-2)+c\right] .\end{aligned}$$

The last integral can be evaluated in a similar fashion as Perram[42] and Barker and Henderson[40,43] have done for the HS correlation function. Differentiating Eq. (A7) three times with respect to x results in an inhomogeneous differential equation in $Z(x)$:

$$\frac{d^3Z}{dx^3}=12\phi\left[ax+b-(a/2+b-c)\frac{d^2Z}{dx^2}+b\frac{dZ}{dx}+aZ\right] \tag{A8}$$

with boundary values

$$\begin{aligned}&Z(1)=P(1) ,\\&\frac{dZ(1)}{dx}=\frac{dP(1)}{dx}+12\phi q(0)Z(1) ,\\&\frac{d^2Z(1)}{dx^2}=\frac{d^2P(1)}{dx^2}+12\phi q(0)\frac{dZ(1)}{dx}+12\phi q'(0)Z(1) ,\\&\frac{d^3Z(1)}{dx^3}=\frac{d^3P(1)}{dx^3}+12\phi q(0)\frac{d^2Z(1)}{dx^2}+12\phi q'(0)\frac{dZ(1)}{dx}\\&\qquad+12\phi q''(0)Z(1) ,\end{aligned} \tag{A9}$$

where $q(0)=-a/2-b+c$, $q'(0)=b$, and $q''(0)=a$. The solution for Z now has the form

$$Z(x)=-x+a_1e^{\mu x}+e^{\eta x}[a_2\cos(\xi x)+a_3\sin(\xi x)] , \tag{A10}$$

where a_1, a_2, and a_3 are obtained by the boundary value equations, μ, η, and ξ are determined by the roots of the characteristic equation of the homogeneous part of the differential equation:

$$\Lambda^3+(a/2+b-c)\Lambda^2-b\Lambda-a=0 . \tag{A11}$$

This equation always has three roots of the form

$$\Lambda_1=\mu,\quad \Lambda_2=\eta+i\xi,\quad \Lambda_3=\eta-i\xi .$$

Equations (A5), (A10), and (A11) give explicitly the solution for $g(x)$ for $0<x<2$. From here on a stepwise solu-

tion for $g(x)$ can be made to obtain the function over the successive intervals $2<x<3$, $3<x<4$, etc. The algebra however becomes rather cumbersome. In this paper we have only need for the expression for $Z(x)$ the range $0<x<2$. However we point out that because $g(x)$ and its derivatives are well behaved (piecewise continuous) for $x>2$ it is possible to apply the efficient algorithm proposed by Glandt and Kofke. This makes use of successive applications of the trapezoidal to solve Eq. (A7) for $Z(x)$ to any required accuracy.[44]

---

*Correspondence address: Department of Molecular Biophysics, University of Utrecht, Buys Ballot Laboratory, P. O. Box 80.000, 3508, TA Utrecht, The Netherlands.

[1]*Micellication, Solubilization and Microemulsions,* edited by K. L. Mittal (Plenum, New York, 1977).

[2]*Surfactants in Solution,* edited K. L. Mittal and B. Lindman (Plenum, London, 1987).

[3]R. Aveyard, B. P. Binks, S. Clark, and J. Mead, J. Chem. Soc. Faraday Trans. I **82**, 125 (1986).

[4]R. Aveyard, B. P. Binks, S. Clark, and J. Mead, J. Chem. Soc. Faraday Trans. I **82**, 1755 (1986).

[5]R. A. Day, B. H. Robinson, J. H. R. Clark, and J. V. Doherty, J. Chem. Soc. Faraday Trans. I **75**, 132 (1979).

[6]M. Zulauf and H. F. Eicke, J. Phys. Chem. **83**, 480 (1978).

[7]M. Kotlarchyk, S. H. Chen, and J. S. Huang, J. Chem. Phys. **86**, 3276 (1982).

[8]M. Kotlarchyk and S. H. Chen, J. Chem. Phys. **79**, 2461 (1983).

[9]T. N. Zemb, S. T. Hyde, P.J. Derian, I. S. Barnes, and B. W. Ninham, J. Phys. Chem. **91**, 3814 (1987).

[10]M. Kotlarchyk, S. H. Chen, J. S. Huang, and M. W. Kim, Phys. Rev. A **29**, 2054 (1984).

[11]J. S. Huang, S. A. Safran, M. W. Kim, G. S. Grest, M. Kotlarchyk, and N. Quirke, Phys. Rev. Lett. **53**, 592 (1985).

[12]J. Lang, A. Jada, and A. Malliaris, J. Phys. Chem. **92**, 1946 (1988).

[13]I. S. Barnes, S. T. Hyde, B. W. Ninham, P. J. Derion, M. Drifford, and T. N. Zemb, J. Phys. Chem. **92**, 2286 (1988).

[14]M. J. Hou, M. Kim, and D. O. Shah, J. Colloid Interface Sci. **123**, 398 (1988).

[15]R. Hilfiker, H. F. Eicke, S. Geiger, and G. Furler, J. Colloid Interface Sci. **105**, 378 (1985).

[16]H. F. Eicke and J. Rehak, Helv. Chim. Acta **59**, 2883 (1976).

[17]M. L. Robbins, J. Boch, and J. S. Huang, J. Colloid Interface Sci. **126**, 114 (1988).

[18]M. A. van Dijk, G. Casteleijn, J. G. H. Joosten, and Y. K. Levine, J. Chem. Phys. **85**, 626 (1986).

[19]M. A. van Dijk, E. Broekman, J. G. H. Joosten, and D. Bedeaux, J. Phys. (Paris) **47**, 727 (1986).

[20]M. A. van Dijk, Phys. Rev. Lett. **55**, 1003 (1985).

[21]M. A. van Dijk, Ph.D. thesis, Rijksuniversiteit Utrecht, 1986.

[22]H. F. Eicke, R. Hilfiker, and H. Thomas, Chem. Phys. Lett. **125**, 295 (1986).

[23]M. Lagües, R. Ober, and C. Taupin, J. Phys. Lett. **39**, 487 (1978).

[24]M. Moka-Ouchane, J. Peyrelasse, and C. Boned, Phys. Rev. A **35**, 3027 (1987).

[25]M. Borkovec, H. F. Eicke, H. Hammerich, and B. Das Gupta, J. Chem. Phys. **92**, 206 (1988).

[26]D. Bedaux, M. M. Wind, and M. A. van Dijk, Z. Phys. B **68**, 343 (1987).

[27]D. A. McQuarrie, *Statistical Mechanics* (Harper & Row, New York, 1976).

[28]C. A. Croxton, *Introduction to Liquid State Theory* (Wiley, New York, 1975).

[29]B. Cabane, in *New Methods of Investigation, Surfactant Science Series,* edited by R. Zana (Marcel Dekker, New York, 1987), Vol. 22.

[30]A. Guinier and G. Fournet, *Small Angle Scattering of X-rays* (Wiley, New York, 1955).

[31]M. Borkovec and H. F. Eicke, Chem. Phys. Lett. **147**, 195 (1988).

[32]M. Borkovec, J. Chem. Phys. **91**, 6268 (1989).

[33]C. Robertus, W. H. Philipse, J. G. H. Joosten, and Y. K. Levine, J. Chem. Phys. **90**, 4482 (1989).

[34]R. Landauer, in *Electrical Transport and Optical Properties of Inhomogeneous Media (Ohio State University, 1977),* Proceedings of the First Conference on the Electrical Transport and Optical Properties of Inhomogeneous Media, AIP Conf. Proc. No. 40, edited by J. S. Garland and D. B. Tanner (AIP, New York, 1978).

[35]R. J. Baxter, J. Chem. Phys. **49**, 2770 (1968).

[36]J. K. Percus and G. J. Yevick, Phys. Rev. **110**, 1 (1958).

[37]H. Kranendonk and D. Frenkel, Mol. Phys. **64**, 40 (1988).

[38]N. A. Seaton and E. D. Glandt, J. Chem. Phys. **86**, 4668 (1987).

[39]C. Regnaut and J. C. Ravey, J. Chem. Phys. **91**, 1211 (1989).

[40]J. A. Barker and D. Henderson, Rev. Mod. Phys. **48**, 587 (1976).

[41]W. R. Smith and D. Henderson, Mol. Phys. **19**, 411 (1970).

[42]J. W. Perram, Mol. Phys. **30**, 1505 (1975).

[43]J. A. Barker and D. Henderson, Mol. Phys. **21**, 187 (1971).

[44]E. D. Glandt and D. A. Kofke, Mol. Phys. **64**, 125 (1988).

[45]R. J. Baxter, J. Chem. Phys. **52**, 4559 (1969).

[46]P. T. Cummings, J. W. Perram and E. R. Smith, Mol. Phys. **31**, 535 (1976).

[47]B. Barboy, Chem. Phys. **11**, 357 (1975).

[48]J. W. Perram and E. R. Smith, Chem. Phys. Lett. **35**, 138 (1975).

[49]G. V. Schulz, Z. Phys. Chem. **43**, 25 (1935).

[50]M. Kotlarchyk, R. B. Stevens, and J. S. Huang, J. Phys. Chem. **92**, 1533 (1988).

[51]L. Blum and G. Stell, J. Chem. Phys. **71**, 42 (1979).

[52]W. L. Griffith, R. Triolo, and A. L. Compere, Phys. Rev. A **35**, 2200 (1987).

[53]P. van Beurten and A. Vrij, J. Chem. Phys. **74**, 2744 (1981).

[54]A. Vrij, J. Chem. Phys. **69**, 1742 (1978).

[55]A. Vrij, J. Chem. Phys. **71**, 3267 (1979).

[56]J. J. Salacuse and G. Stell, J. Chem. Phys. **77**, 3714 (1982).

[57]C. Robertus, J. G. H. Joosten, and Y. K. Levine, Prog. Colloid Polym. Sci. **77**, 115 (1988).

[58]D. W. Marquardt, J. Soc. Ind. Appl. Math. **11**, 431 (1963).

[59]P. Ekwall, L. Mandel, and K. Fontell, J. Colloid Interface Sci. **33**, 215 (1970).

[60]S. M. F. Tavenier, Ph.D. thesis, Universiteit Antwerpen, 1981.